



Check for updates



High-Throughput PV Module Diagnostics using a Compact NIR Spectrometer

Oleksandr Mashkov 📵 | Lewin Leihkamm | Oleksandr Stroyuk | Claudia Buerhop | Thilo Winkler | Ones Ghaffari | Stefanie Vorstoffel | Ernst Wittmann | Jens Hauch | Ian Marius Peters

Helmholtz-Institut Erlangen Nürnberg für Erneuerbare Energien (HI ERN), Forschungszentrum Jülich GmbH, Erlangen, Germany

Correspondence: Oleksandr Mashkov (o.mashkov@fz-juelich.de)

Received: 29 April 2025 | Revised: 21 July 2025 | Accepted: 1 August 2025

Funding: German Federal Ministry for Economic Affairs and Climate Action, "dig4morE", Grant/Award Number: 03EE1090B; Helmholtz Association in the framework of the innovation platform, "Solar TAP", Grant/Award Number: 714-62150-3/1; German Federal Ministry for Economic Affairs and Climate Action, "REMBup", Grant/Award Number: FKZ03EWR021F

Keywords: backsheet polymers | chemometric analysis | compact spectrometer | field diagnostics | near-infrared spectroscopy | photovoltaics | recycling

ABSTRACT

The degradation of backsheets and encapsulants in photovoltaic (PV) modules compromises their long-term performance and reliability. This study investigates the use of a compact near-infrared (NIR) spectrometer for high-throughput field diagnostics of PV materials. Operating in the 1550–1950 nm spectral range, the spectrometer detects key molecular absorption bands to characterize polymer compositions. Principal component analysis (PCA) applied to the spectral data significantly improved material differentiation compared to raw data, achieving classification reliability exceeding 95%. Field deployment at a 10 mw PV installation demonstrated the method's scalability, with 981 modules analyzed at a rate of one module every 3 s. Spatial mapping revealed that all analyzed backsheets featured polyethylene terephthalate (PET) cores, with approximately 65% incorporating fluoropolymer- and 35% PET-based outer layers. These findings demonstrate the scalability and efficiency of a portable NIR spectrometer for rapid, nondestructive diagnostics of PV modules. The ability to directly identify polymer compositions during high-throughput field measurements enables applications in predictive maintenance, reliability assessment, bill-of-materials verification, and efficient sorting and recycling of end-of-life modules.

1 | Introduction

The deployment of photovoltaic (PV) systems has become a global priority in the transition toward sustainable energy solutions. The long-term reliability of the field-installed PV modules depends on the degradation of their constituent components. Backsheets and encapsulants play crucial roles in protecting solar cells from environmental stresses such as ultraviolet (UV) radiation, moisture ingress, and helping to reduce thermal gradients. Degradation of backsheets and encapsulants compromises the structural and electrical integrity of PV modules and affects their overall energy yield and operational safety [1–3].

Backsheets are typically composed of three-layered polymer stacks, with a polyethylene terephthalate (PET) core sandwiched between outer layers made of materials such as polyvinylidene fluoride (PVDF), polyvinyl fluoride (PVF), fluorinated copolymers, polyethylene (PE), and polypropylene (PP). These multilayer structures exhibit distinct aging behaviors under prolonged environmental exposure.

Similarly, encapsulants, such as ethylene-vinyl acetate (EVA) copolymer or more modern polyolefin elastomers (POE), are prone to hydrolytic and photothermal degradation, which can lead to material failure over time. Considering that the polymer bill-of-materials of installed PV modules are often nondisclosed

This is an open access article under the terms of the Creative Commons Attribution License, which permits use, distribution and reproduction in any medium, provided the original work is properly cited.

© 2025 The Author(s). Solar RRL published by Wiley-VCH GmbH.

or not traceable, identifying these polymer materials in the field and monitoring their degradation pathways are essential for improving module design and developing adequate maintenance strategies [4–6].

Spectroscopic methods, particularly near-infrared (NIR) spectroscopy, have proven effective in characterizing polymer backsheets and encapsulants. NIR spectroscopy enables rapid, nondestructive analysis of molecular vibrational features of polymer stacks with thicknesses of many hundreds of microns, making it ideal for nondestructive identification of polymer types [7].

Traditional laboratory-based Fourier-transform near-infrared (FT-NIR) spectrometers offer high resolution and sensitivity but are often impractical for field applications due to their size/price, the complexity of their operation, and the sensitivity of these methods to climatic conditions. To address these limitations, compact and robust handheld NIR spectrometers have been tested, allowing in-situ field analysis of polymeric materials in PV modules [8]. However, the miniaturization of the spectrometer leads to certain trade-offs, particularly in spectral resolution and signal-to-noise ratio, which can affect measurement accuracy and material differentiation. While a compact NIR spectrometer offers the advantage of portability and robustness, its reliability in field applications compared to high-performance laboratory systems remains an open question. In particular, challenges such as calibration stability, measurement consistency, and spectral interference must be addressed to ensure their effectiveness in real-world diagnostics.

This study aims to evaluate the performance of a miniature handheld near-infrared spectrometer (NIRONE S2.0 by Spectral Engines) for identifying PV polymer compositions. In contrast to our previous studies [9, 10] that focused on laboratory-scale validation, this work demonstrates the transition of NIR spectroscopy into a robust, high-throughput field tool. The device's capabilities are tested in both laboratory and field environments and benchmarked against a high-end benchtop FT-NIR spectrometer (ARCoptix FTNIR-L1-026-0TE) to compare measurement accuracy, resolution, and practical applicability. To ensure reliable classification despite reduced spectral resolution and increased noise, a tailored preprocessing workflow was applied, including baseline correction and selective exclusion of water absorption bands. The compact NIR spectrometer

integrates portability with consistent and reliable data acquisition, enabling rapid, noninvasive field diagnostics, with measurement times of approximately 3 s per module and deployment across nearly 1000 PV modules. By detecting spectral variations associated with polymer degradation, this study examines the sensor's capability for backsheet identification and degradation monitoring. The results provide meaningful insight into its suitability for high-throughput PV diagnostics and its potential role in predictive maintenance strategies, as recent field studies show that bill-of-materials (BOM) identification enables early detection of degradation-prone materials, such as PA or FC backsheets and specific EVA types, which are linked to insulation loss, potential-induced degradation (PID), and inverter shutdowns [11–15]. More broadly, this approach supports future integration into semiautomated and machine learning-driven diagnostic platforms alongside thermography, UV fluorescence, and photoluminescence imaging.

2 | Description of NIR Spectrometers

Near-infrared absorption (NIRA) measurements were performed using the NIRONE S2.0 sensor (Spectral Engines, Finland) to analyze commercial solar PV modules with glass-backsheet architectures. Its compact design enables noninvasive, high-throughput field measurements. Although limited to the 1550–1950 nm spectral range, the sensor detects key molecular absorption bands corresponding to C–H bonds in aromatic and aliphatic compounds and O–H bonds indicative of water content. This spectral window was specifically selected for backsheet identification, while encapsulant analysis in glass/glass modules remains ongoing. Measurements were performed in NIR reflectance mode, and NIRA spectra were calculated using the reflectance spectrum of the NIR excitation source detected with a Spectrolon standard provided by the manufacturer.

For reference, a fiber-coupled FT-NIR spectrometer (FTNIR-L1-026-0TE, ARCoptix, Switzerland) was used. This benchtop mirror interferometer-based system provides a larger spectral range (900–2600 nm), but requires an external light source and power supply, making potential field deployment more complex. A direct comparison of key specifications is presented in Table 1, ensuring consistency in performance metrics:

TABLE 1 | Comparison of NIRONE and ARCoptix FT-NIR spectrometers.

Specification	NIRONE S2.0 (spectral engines)	FT-NIR (ARCoptix)
Spectral range [nm]	1550–1950 nm	900–2600 nm
Resolution	1–10 nm	<1 nm
Detector type	Single-element extended InGaAs	Extended InGaAs
Signal-to-noise ratio (SNR)	11 000 - 1500	>30 000:1
Power consumption	<1.1 W (peak) < 300 mW (nominal)	7.5–12V (1–6W depending on version)
Operating temperature [°C]	+10 to +50	+5 to +35
Built-in NIR light source	Yes	No
Size (W \times L \times H), mm	$25 \times 25 \times 17.5$	$180 \times 126 \times 78$
Weight, g	15	1700

3 | Identifying Backsheet Compositions through Characteristic Spectral Patterns

3.1 | Spectral Data Acquisition and Challenges

Before field deployment, the miniature NIR spectrometer needs to be calibrated in the lab using a collection of known backsheet types. This lab-based study investigated field-aged solar modules with six distinct backsheet types (Table 2) from different manufacturers [10].

The spectral data for different backsheets were collected using the NIRONE spectrometer, which operates at a lower resolution compared to the ARCoptix device (Figure 1). Despite this limitation, the NIRONE spectra capture key absorption bands associated with backsheet polymers, including the first overtone of =C-H vibration at 1660 nm, an overtone of -C-H vibration at 1730 nm, and the O-H vibration band at 1910 nm (Figure 2a).

At first glance, the spectra show significant differences, further complicated by additional factors. In particular, variations in backsheet compositions due to aging, weather exposure, and manufacturing differences introduce sample heterogeneity [16–18]. Instrumental artifacts, such as noise and distortions

TABLE 2 | Backsheet structures used for the lab-based calibration and their abbreviations.

Structure	Abbreviation
PET/PET/PE	$A^{\rm PET}$
PVF1/PET/PVF1	B^{PVF}
PA	C^{PA}
PVDF/PET/PVDF	$\mathrm{D}^{\mathrm{PVDF}}$
PVF2/PET/PVF2	$\mathrm{E}^{\mathrm{PVF}}$
FC/PET/FC	F^{FC}

Notes: Indices (1) and (2) refer to different thicknesses, $50-55 \mu m$ for (1), and $30-35 \mu m$ for (2); the air layer and the inner layer of backsheets are typically filled with microcrystalline rutile titania pigments.

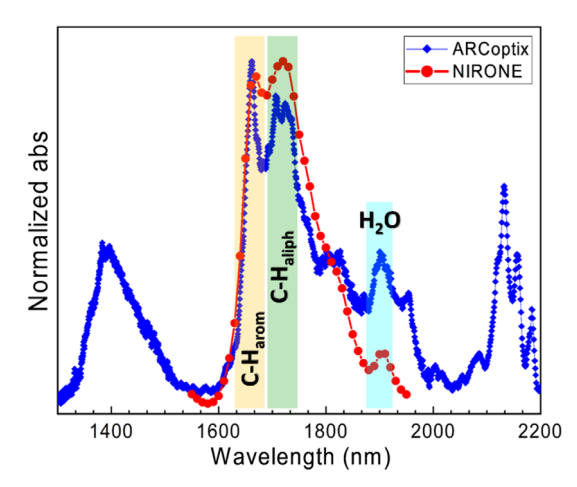


FIGURE 1 | Comparison of normalized NIRA spectra from ARCoptix (diamond scatter) and NIRONE (circle scatter) spectrometers for an exemplary F^{FC} backsheet.

caused by the spectrometer's hardware, also affect the data. Additionally, scattering effects from additives like rutile ${\rm TiO_2}$ pigments, which are often present in backsheets, contribute to the complexity and variability of the NIRA spectra. Environmental factors can further alter the spectral results [16]. These combined influences make it challenging to directly associate the raw spectral data with specific backsheet types. The overlapping features and broad absorption bands obscure the differences between different materials in the polymer stack forming the backsheet, preventing clear differentiation.

Since the handheld sensor has a lower spectral resolution and higher noise levels, the raw spectra show broad, overlapping absorption bands that limit the ability to reliably distinguish between different backsheet types. To resolve this ambiguity, advanced preprocessing coupled with dimensionality reduction techniques, such as principal component analysis (PCA), was applied to extract meaningful chemical information for accurate backsheet classification. The preprocessing steps included baseline correction and exclusion of the water absorption band, as discussed in the following sections.

3.2 | PCA for Backsheet Differentiation

To overcome challenges in raw spectral data interpretation, PCA [19] was applied to the spectral data collected by the NIRONE spectrometer. When applied to unprocessed spectral data, PCA successfully separated the six backsheet types into distinct clusters (Figure 2b). The PCA outcomes, including the first two principal components, PC1 and PC2, accounting for 98.74% and 0.76% of the total variance, respectively, and clustering indices are presented in Table 3.

To evaluate the reliability of the classification, several clustering indices were applied. The Silhouette Score [20] measures how well points fit within their clusters (higher values indicate better clustering), while the Davies-Bouldin index (DBI) [21] evaluates cluster separation (lower values indicate higher reliability). The Calinski-Harabasz index (CHI) [22] quantifies cluster compactness relative to separation (higher values indicate well-defined clusters). These metrics, typically applied to evaluate clustering algorithms [23, 24] such as K-means, hierarchical clustering, density-based or distribution-based methods, can also be used to assess the separation of predefined classes in PCA [25-28] space. Here, they quantify how distinctly different backsheet types form separable groups in the reduced spectral feature space. Applied in this way, the clustering metrics provide a robust and interpretable measure of classification quality. The dominance of PC1 suggests that most spectral variance is due to baseline effects or instrumental noise, whereas the minimal contribution of PC2 indicates that only a small portion of variance corresponds to the chemical composition of the backsheet sample. Optimizing clustering performance increases the separation between backsheet types by minimizing the influence of artifacts, instrumental noise, and baseline variations. This ensures that classification is driven by meaningful spectral features, resulting in more distinct and reliable groupings.

To investigate the reasons for the large imbalance between PC1 and PC2, an advanced analysis of the raw spectra was further

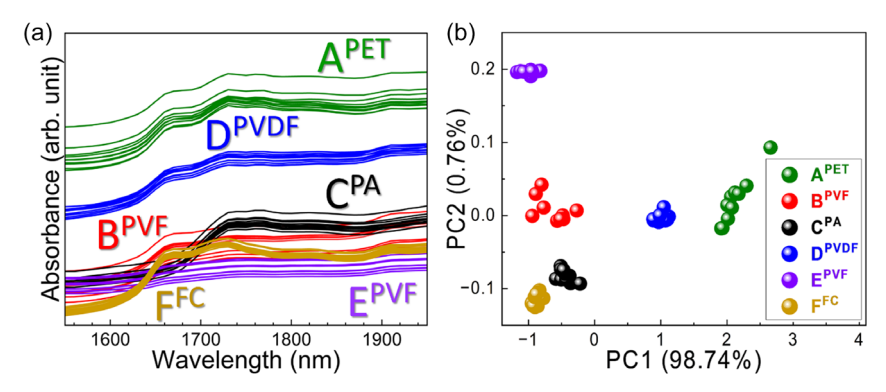


FIGURE 2 | NIRA spectra and PCA analysis of spectral data: a) raw absorbance spectra of six backsheet types and b) PCA of unprocessed spectral data.

TABLE 3 | Clustering metrics for spectral data.

	Silhouette score (S)	Davies-Bouldin index (DBI)	Calinski– Harabasz index (CHI)
Raw absorbance data (1550-1950nm)	0.61	0.64	770.81
Processed data (1550-1950nm)	0.78	0.31	1706.28
Processed data without H ₂ O band (1550–1890nm)	0.74	0.33	1886.82

performed. It was hypothesized that baseline effects, such as instrument drift or background interference mask important spectral features, leading to the dominance of PC1 that may not reflect meaningful chemical variations. This imbalance is problematic because it suggests that most variance in the data is driven by noninformative factors rather than actual differences in backsheet composition, potentially reducing classification accuracy.

To account for this effect, a baseline correction was applied to remove spectral background signals, revealing true absorption features (Figure 3a and S1a). After baseline correction, spectra were integrated into the range of 1550–1950 nm to obtain a representative value for each backsheet type, revealing distinct absorption patterns (Figure 3a). This correction significantly improved data clarity, making it easier to differentiate backsheet types.

Additionally, the baseline integral over 1550-1950 nm was calculated to quantify its contribution to spectral features. The corrected spectra were then divided into four absorption regions: 'aromatic' = C-H band [29] (1570-1700 nm), 'aliphatic' - C-H band (1700-1750 nm), a scattering-dominated region (1750-1850 nm, chemically meaningless), and water-related absorption (1850-1950 nm), the latter indicating possible moisture ingress. The integrals of these spectral regions were compared across the six backsheet types, revealing the 1700-1750 nm range as particularly significant for distinguishing between different backsheets by baseline area (Figure 3b). PCA score analysis revealed that PC1 corresponded to baseline integrals, reflecting background effects rather than meaningful spectral content, while PC2 was related to the 1700-1750 nm region, capturing aliphatic bond-related features. These findings highlight that PC1, despite accounting for most variance, is largely noninformative. Removing the baseline before PCA significantly improves

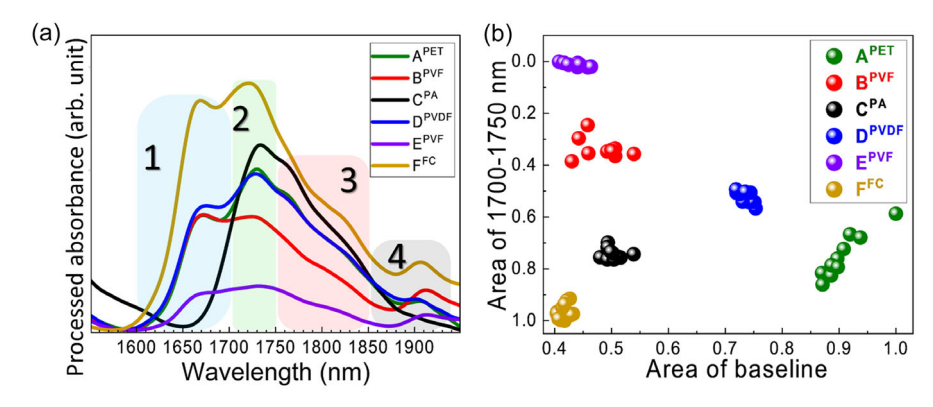


FIGURE 3 | Processed spectra and feature-based clustering: a) identification of key absorption features, and b) 2D clustering based on the relationship between baseline area and peak area in the 1700–1750 nm range.

analysis relevance by ensuring that the variance reflects actual chemical differences rather than artifacts (Figure 4a). This conclusion is supported by clustering metrics: the Silhouette Score increased from 0.61 to 0.78, the DBI decreased from 0.64 to 0.31, and the CHI more than doubled from 770.81 to 1706.28, indicating substantially improved cluster separation and reliability of classification (Table 3).

To assess the impact of spectral preprocessing on classification accuracy, integrals for the identified spectral regions were recalculated, and a new mapping approach was implemented. As a result, the contribution of PC1 and PC2 became more balanced compared to unprocessed data, with improved clustering indices (Table 3), indicating a clearer separation of backsheet types. The integral map (Figure S1b) showed that plotting 'aromatic' (1570-1700 nm) versus 'aliphatic' (1700-1750 nm) integrals mimics PCA clustering, confirming that PCA effectively represents the ratio of these vibrational intensities in polymer backsheets. Loadings analysis (Figure 4b) further validated these findings by identifying spectral regions that contributed most to each principal component. In particular, PC1 was primarily influenced by =C-H band intensity, while PC2 reflected aliphatic -C-H vibrations, reinforcing their significance in backsheet differentiation [19]. The improved separation between backsheet types demonstrates that the spectral preprocessing applied successfully extracts relevant chemical information.

A key consideration in the spectral analysis was the presence of water absorption in the 1850–1950 nm range. Since some polymeric backsheets—particularly nonfluorinated types—can absorb

moisture [30] depending on environmental conditions [31], their spectral NIRA signatures may be affected by transient water content, independently of material composition. In contrast, fluorinated layers typically exhibit low moisture uptake but may still allow limited water permeation. The influence of transient environmental factors on PCA classification can be considerably reduced by neglecting the water absorption band during the spectral analysis. To evaluate the impact of water absorption on classification accuracy, the spectral region highlighted in Figure S2, where water bands are present, was analyzed. These absorption bands may result from moisture retention within the polymer matrix due to its porosity and physicochemical interactions with water. To determine whether this region influenced PCA classification, this water-related range was excluded, and the remaining data (Region 1 in Figure S2) were reanalyzed using PCA (Figure 4c). The results in Figure 4c indicate that excluding the water absorption band did not alter the clustering patterns. Moreover, the percentage contributions of PC1 and PC2, 81.06% and 16.45%, respectively, as well as the clustering indices (DHI and CHI, Table 3), remained consistent, suggesting that water presence does not significantly impact the classification of backsheet types.

To further validate the robustness of the clustering, confidence ellipses [32] were applied to the PCA space (Figure 4c) to assess assignment probability and cluster separation. These ellipses represent probability regions corresponding to 1σ (68.27%), 2σ (95.45%), and 3σ (99.73%) uncertainty levels, based on a multivariate Gaussian distribution [33, 34] for each cluster. Assignment was performed by evaluating whether a sample fell within the 2σ

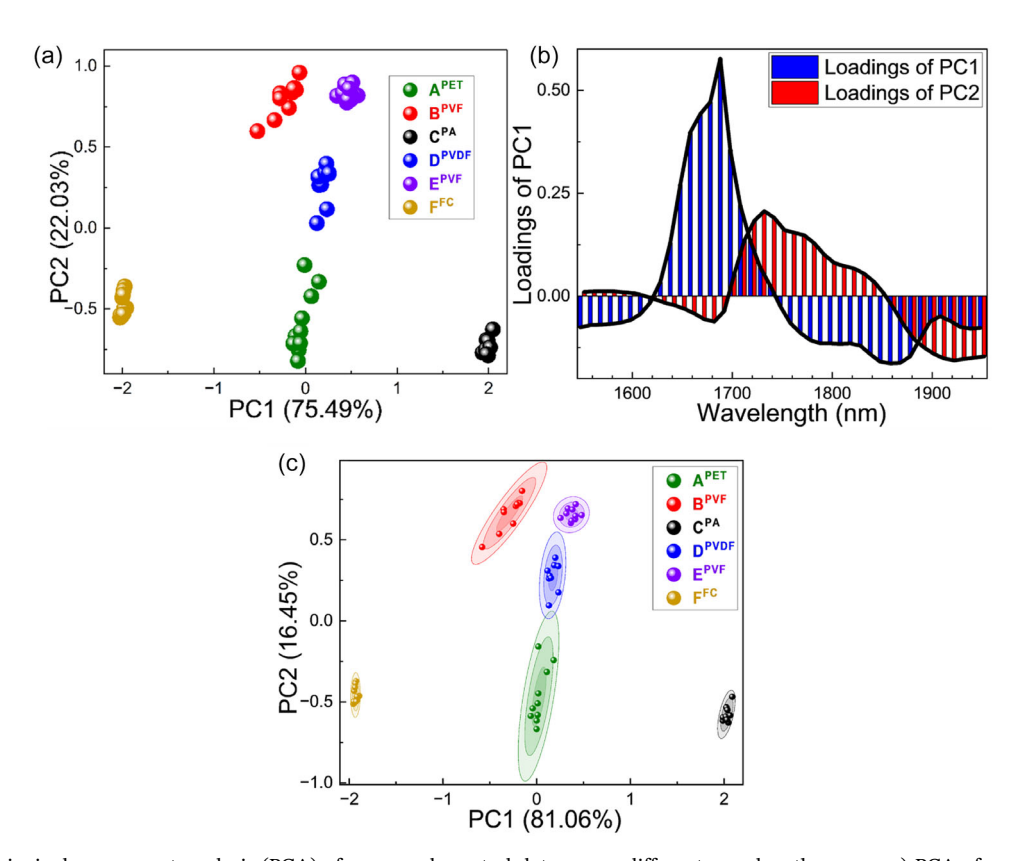


FIGURE 4 | Principal component analysis (PCA) of processed spectral data across different wavelength ranges: a) PCA of processed data (1550–1950 nm), b) loading spectra of PC1 and PC2, and c) PCA of data excluding the water band (1550–1890 nm) with confidence ellipses.

ellipse of a known cluster; samples lying outside the 3σ ellipses were considered unassigned. This approach allows visualization of cluster spread and overlap, and enables quantitative assessment of classification reliability based on Mahalanobis distance.

These results confirm that, following appropriate preprocessing, the NIRONE spectrometer enables reliable differentiation of backsheet types with high classification confidence, even under varying environmental conditions.

4 | Field Testing of NIRONE Sensor in Solar Plants

To assess the performance of the NIRONE sensor in field conditions, it was deployed at a large-scale PV plant in Southern Germany with a capacity of 10 MWp and a commissioning age of more than 10 years. The primary objective was to identify different backsheet types and compare the outcomes of measurements with NIRONE to those obtained using the high-end ARCoptix spectrometer as a reference. The evaluation focused on classification accuracy, measurement speed, and practical usability.

The ARCoptix system was employed to measure three rows of solar modules, resulting in spectral data from 127 modules, with each measurement taking approximately 2 min per module. The acquisition time was determined by the need to manually move a carriage containing the spectrometer, NIR lamp, fiber-coupled probes, and power supply along the row of PV modules before each measurement. In contrast, the NIRONE sensor, optimized for high-throughput measurements, was used to test 981 modules across the PV plant, with a significantly shorter acquisition time of ca. 3 s per module. This shorter acquisition time is enabled by the integration of the NIR lamp into the spectral sensor and the use of a tablet PC for power supply, allowing an experimenter to move freely along the row of PV modules.

As discussed in previous sections, the spectral range of the NIRONE sensor was 1550–1950 nm, specifically selected for backsheet identification (Figure 1). The initial analysis demonstrated that both the ARCoptix and NIRONE systems effectively differentiated between two backsheet types: PET/PET/PE (A $^{\rm PET}$) and FC/PET/FC (F $^{\rm FC}$) present in the test field, see Figure S3a, b (SI). However, while both systems provided reliable classification, the NIRONE sensor enabled a much higher sampling rate, allowing for a more comprehensive mapping of backsheet distribution across the PV plant for the same measurement period.

The backsheet identification model developed in this study (see Section 3.2) was applied to generate a spatial distribution map of backsheet types (Figure 5). The results showed that rows 1–9 and 11 predominantly consisted of F^{FC} backsheets, while rows

10 and 12 were primarily composed of A^{PET} backsheets. Classification was performed using confidence ellipses derived from PCA space, with most data points falling within the 2σ (95.45% confidence) region, corresponding to a squared Mahalanobis distance (d²) threshold of 5.99, as defined by the chi-squared (χ ²) distribution with 2° of freedom. This indicates a high degree of reliability in the assignment of backsheet types across the analyzed modules.

Notably, the NIRONE sensor demonstrated stable operation across a broad temperature range, up to 60°C, and a long operational time, allowing all modules to be probed without additional recharging of the sensor-tablet combination.

5 | Conclusion

This study explored the application of a compact NIR spectrometer for high-throughput PV module diagnostics, focusing on backsheet identification and classification. By leveraging PCA and spectral preprocessing, the NIRONE spectrometer successfully differentiated between six distinct backsheet types. Clustering metrics confirmed improved classification accuracy, with the Silhouette Score increasing from 0.61 to 0.78, the DBI decreasing from 0.64 to 0.31, and the CHI rising from 770 to 1706 after baseline correction. These improvements indicate that baseline correction reduced noninformative spectral variance, enhanced cluster separation, and increased the compactness of distinct backsheet groups in PCA space.

The final PCA was further optimized by applying baseline correction and calculating spectral integrals over key absorption regions. Excluding the water absorption band (1850–1950 nm) confirmed that moisture variability did not affect classification. The final model used the 1550–1950 nm range, focusing on absorption bands of aromatic (1570–1700 nm) and aliphatic species (1700–1750 nm), instrumental for backsheet differentiation. Confidence ellipses were applied to PCA clustering to assign new data points to existing clusters, enabling the visualization of cluster spread and overlap.

Field testing at a 10 MWp PV plant covered 981 modules, with the NIRONE sensor measuring each in 3 s, compared to 2 min per module for the high-end ARCoptix system. A spatial distribution map was generated, visualizing the populations of two backsheet types, FC/PET/FC and PET/PET/PE, in full agreement with the results obtained from the reference high-end ARCoptix NIR spectrometer. This one-to-one correspondence across all tested modules confirms the reliability of the NIRONE sensor for large-scale diagnostics.

These findings demonstrate the potential of a compact NIR spectrometer for efficient polymer characterization in PV systems. Their fast performance, portability, robustness, and nondestructive

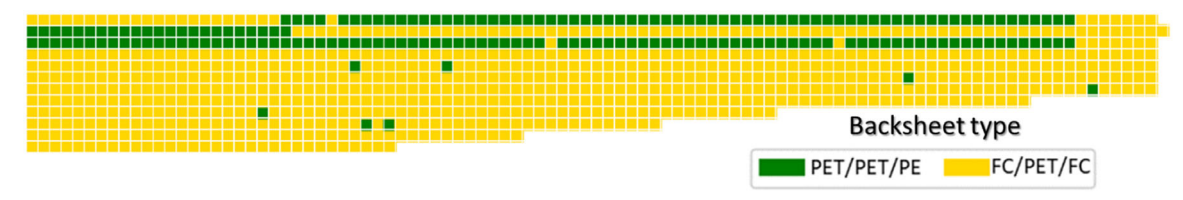


FIGURE 5 | Spatial distribution of backsheet types across the tested PV plant.

measurement capability allow for rapid assessment of backsheet structures. Future work may focus on refining classification models, expanding spectral range, and integrating machine learning to enhance accuracy and predictive capabilities in PV module diagnostics, while also enabling more efficient sorting and recycling of end-of-life modules through improved polymer identification.

Acknowledgments

This work is supported by the German Federal Ministry for Economic Affairs and Climate Action ("dig4morE", No. 03EE1090B, "REMBup" FKZ 03EWR021F) and the Helmholtz Association in the framework of the innovation platform "Solar TAP" (No. 714-62150-3/1 (2023)). Views and opinions expressed are, however, those of the author(s) only and do not necessarily reflect those of the European Union or the European Research Council. Neither the European Union nor the granting authority can be held responsible for them. All authors contributed equally to this work.

Open Access funding enabled and organized by Projekt DEAL.

Conflicts of Interest

The authors declare no conflicts of interest.

Data Availability Statement

The data that support the findings of this study are available from the corresponding author upon reasonable request.

References

- 1. B. Mohamed, S. Zambou, and S. S. Zekeng," *Influence of Moisture on the Operation of a Mono-Crystalline Based Silicon Photovoltaic Cell: A Numerical Study Using SCAPS 1 D*," (2017), https://doi.org/10.48550/arXiv.1712.08117.
- 2. C. Buerhop, T. Pickel, O. Stroyuk, J. Hauch, and I. M. Peters, "An Insight into a Combined Effect of Backsheet and EVA Encapsulant on Field Degradation of PV Modules," *Energy Science & Engineering* 11, (2023): 4168–4180.
- 3. D. E. Mansour, C. Barretta, L. Pitta Bauermann, et al., "Effect of Backsheet Properties on PV Encapsulant Degradation during Combined Accelerated Aging Tests," *Sustainability* 12, (2020): 5208.
- 4. N. T. Dintcheva, E. Morici, and C. Colletti, "Encapsulant Materials and Their Adoption in Photovoltaic Modules A Brief Review," *Sustainability* 15, (2023): 9453.
- 5. Y. Wang, et al., "Degradation Models of Photovoltaic Module Backsheets Exposed to Diverse Real World Condition," in 2017 IEEE 44th Photovoltaic Specialist Conference (PVSC), (IEEE, 2017), 2000–2004, https://doi.org/10.1109/PVSC.2017.8366636.
- 6. C. Barretta, G. Oreski, S. Feldbacher, K. Resch-Fauster, and R. Pantani, "Comparison of Degradation Behavior of Newly Developed Encapsulation Materials for Photovoltaic Applications under Different Artificial Ageing Tests, *Polymers* 13, (2021): 271.
- 7. O. Stroyuk, C. Buerhop-Lutz, A. Vetter, J. Hauch, and C. J. Brabec, "Nondestructive Characterization of Polymeric Components of Silicon Solar Modules by Near-Infrared Absorption Spectroscopy (NIRA)," Solar Energy Materials and Solar Cells 216, (2020): 110702.
- 8. R. F. Kranenburg, Y. Weesepoel, M. Alewijn, "The Importance of Wavelength Selection in on-Scene Identification of Drugs of Abuse with Portable Near-Infrared Spectroscopy," *Forensic Chemistry* 30, (2022): 100437.
- 9. O. Stroyuk, C. Buerhop-Lutz, J. Hauch, and I. M. Peters, "Solar-NIRT: Identification of PV-Module Backsheets in the Field with Natural

- Sunlight," Progress in Photovoltaics: Research and Applications 30, (2022): 851–858.
- 10. O. Stroyuk, C. Buerhop-Lutz, A. Vetter, et al., "Distinguishing between Different Types of Multi-Layered PET-Based Backsheets of PV Modules with Near-Infrared Spectroscopy," *Progress in Photovoltaics: Research and Applications* 30, (2022): 859–868.
- 11. C. Buerhop, O. Stroyuk, J. Zöcklein, T. Pickel, J. Hauch, and I. M. Peters, "Wet Leakage Resistance Development of Modules with Various Backsheet Types," *Progress in Photovoltaics: Research and Applications* 30, (2022): 938–947.
- 12. F.ibne Mahmood and G. TamizhMani, "Impact of Different Backsheets and Encapsulant Types on Potential Induced Degradation (PID) of Silicon PV Modules," *Solar Energy* 252, (2023): 20–28,
- 13. C. Buerhop Lutz, L. Lüer, O. Stroyuk, J. Hauch, and I. M. Peters, "Dynamics of Backsheet-Driven Insulation Issues," *Solar Energy Materials and Solar Cells*257, (2023): 113898.
- 14. C. Buerhop-Lutz, O. Stroyuk, J. A. Hauch, and I. M. Peters, "Impact of Backsheet Variety on Inverter Availability," *IEEE Journal of Photovoltaics* 14, (2024): 53–58.
- 15. C. Buerhop-Lutz, T. Pickel, O. Stroyuk, J. Hauch, and I. M. Peters, "Insulation Resistance in Relation to Distribution of Backsheet Types in Strings and Inverters," *Solar Energy Materials and Solar Cells* 246, (2022): 111913.
- 16. R. J. Barnes, M. S. Dhanoa, and S. J. Lister, "Standard Normal Variate Transformation and De-Trending of Near-Infrared Diffuse Reflectance Spectra, *Applied Spectroscopy* 43, (1989): 772–777.
- 17. G. Oreski, A. Macher, and K. Resch-Fauster, "Low Temperature Induced Physical Aging Effects of Backsheet Materials," in 2021 IEEE 48th Photovoltaic Specialists Conference (PVSC) (IEEE, 2021), 0818–0821, https://doi.org/10.1109/PVSC43889.2021.9518999.
- 18. A. M. C. Davies, "Always Look at the Spectrum: Part 1," NIR Noise Spectra Spectroscopy Europe 23, (2011): 24.
- 19. I. T. Jolliffe and J. Cadima, "Principal Component Analysis: A Review and Recent Developments," *Philosophical Transactions. Series A, Mathematical, Physical, and Engineering Sciences* 374, (2016): 20150202.
- 20. P. J. Rousseeuw, "Silhouettes: A Graphical Aid to the Interpretation and Validation of Cluster Analysis," *Journal of Computational and Applied Mathematics* 20, (1987): 53–65.
- 21. D. L. Davies and D. W. Bouldin, "A Cluster Separation Measure," in IEEE Transactions on Pattern Analysis and Machine Intelligence, Vol. PAMI-1 (1979): 224–227, https://doi.org/10.1109/TPAMI.1979.4766909.
- 22. T. Caliński and J. Harabasz, "A Dendrite Method for Cluster Analysis," *Communications in Statistics* 3, (1974): 1–27.
- 23. Z.-Y. Lim, L.-Y. Ong, and M.-C. Leow, "A Review on Clustering Techniques: Creating Better User Experience for Online Roadshow," *Future Internet* 13, (2021): 233.
- 24. M. Kossakov, A. Mukasheva, G. Balbayev, S. Seidazimov, D. Mukammejanova, and M. Sydybayeva, "Quantitative Comparison of Machine Learning Clustering Methods for Tuberculosis Data Analysis, *Engineering Proceedings* 60, (2024): 20.
- 25. Y. Huang, Y. Liu, P. A. D. Steel, et al., "Deep Significance Clustering: A Novel Approach for Identifying Risk-Stratified and Predictive Patient Subgroups," *Journal of the American Medical Informatics Association: JAMIA* 28, (2021): 2641–2653.
- 26. V. Divya and K. N. Devi, "An Efficient Approach to Determine Number of Clusters Using Principal Component Analysis," in 2018 International Conference on Current Trends towards Converging Technologies (ICCTCT) (IEEE, 2018), 1–16, https://doi.org/10.1109/ICCTCT.2018.8551182.
- 27. G. Wang, Z. Wang, W. Chen, and J. Zhuang, "Classification of Surface EMG Signals Using Optimal Wavelet Packet Method Based on Davies-

Bouldin Criterion," *Medical and Biological Engineering and Computing* 44, (2006): 865–872.

- 28. F. W. Mauldin, H. T. Zhu, R. H. Behler, T. C. Nichols, and C. M. Gallippi, "Robust Principal Component Analysis and Clustering Methods for Automated Classification of Tissue Response to ARFI Excitation," *Ultrasound in Medicine & Biology* 34, (2008): 309–325.
- 29. T. Otto, R. Saupe, A. Weiss, et al., "Dual-Detector Optical MEMS Spectrum Analyzer: Advances, Applications, and Prospects," in Proceedings SPIE 6887, MOEMS and Miniaturized Systems VII, 68870D (February 11, 2008), https://doi.org/10.1117/12.768356.
- 30. G. C. Eder, Y. Voronko, M. Knausz, G. Oreski, T. Koch, and K. A. Berger, "Permeation of Water Vapour Oxygen and Acetic Acid through PV-Backsheets: Correlation with Material Properties and Ageing Induced Changes," *EU PVSEC* (2015).
- 31. M. Knausz, G. Oreski, G. C. Eder, et al., "Degradation of Photovoltaic Backsheets: Comparison of the Aging Induced Changes on Module and Component Level," *Journal of Applied Polymer Science* 132, (2015): 42093.
- 32. R. Johnson, R. A. Johnson, and D. W. Wichern, Applied Multivariate Statistical Analysis (Pearson, 2013).
- 33. T. W. Anderson, An Introduction to Multivariate Statistical Analysis (Wiley, 2003).
- 34. D. F. Morrison, Multivariate Analysis, Overview, in Encyclopedia of Biostatistics (John Wiley & Sons, Ltd., 2005).

Supporting Information

Additional supporting information can be found online in the Supporting Information section. **Figure S1**. a) Baseline in the absorbance spectrum of F^{FC} measured by the NIRONE spectrometer. b) Cluster plot of integral values for the spectral regions 1570–1700 nm and 1700–1750 nm across different backsheet types. **Figure S2**. Absorbance spectra highlighting key regions measured by NIRONE for six different backsheets. **Figure S3**. Absorbance spectra measured across solar modules using different spectrometers. a) Full-range absorbance spectra (1250–2200 nm) of 127 solar modules measured using the ARCoptix spectrometer, b) Absorbance spectra (1550–1950 nm) of 981 solar modules measured using the NIRONE spectrometer.